Self-Protected Thermometry with Infrared Photons and Defect Spins in Silicon Carbide

Yu Zhou,[1] Junfeng Wang,[1] Xiaoming Zhang,[1] Ke Li,[1] Jianming Cai,[2,*] and Weibo Gao[1,3,4,†]

[1]*Division of Physics and Applied Physics, School of Physical and Mathematical Sciences, Nanyang Technological University, Singapore 637371, Singapore*

[2]*School of Physics & Center for Quantum Optical Science, Huazhong University of Science and Technology, Wuhan 430074, People's Republic of China*

[3]*MajuLab, CNRS–Université de Nice-NUS-NTU International Joint Research Unit UMI 3654, Singapore, Singapore*

[4]*The Photonics Institute and Centre for Disruptive Photonic Technologies, Nanyang Technological University, 637371 Singapore, Singapore*

(Received 11 April 2017; revised manuscript received 27 August 2017; published 25 October 2017)

Quantum sensors with solid-state spins have attracted considerable interest due to their advantages in high sensitivity and high spatial resolution. The robustness against environmental noise is a critical requirement for solid-state spin sensors. In this paper, we present a self-protected infrared high-sensitivity thermometry based on spin defects in silicon carbide. Based on the conclusion that the Ramsey oscillations of the spin sensor are robust against magnetic noise due to a self-protected mechanism from the intrinsic transverse strain of the defect, we experimentally demonstrate the Ramsey-based thermometry. The self-protected infrared silicon-carbide thermometry may provide a promising platform for high sensitivity and high-spatial-resolution temperature sensing in a practical noisy environment, especially in biological systems and microelectronics systems.

DOI: 10.1103/PhysRevApplied.8.044015

I. INTRODUCTION

The ever-increasing demand of noninvasive, precise, and high-spatial-resolution thermometers working in many areas of modern science and technology has inspired researchers to develop new techniques to realize this target [1]. In particular, a thermometer capable of subdegree temperature sensitivity combined with integration within a living system could provide a powerful new tool in many areas of biological, physical, and chemical research [1,2]. In recent years, several thermometry methods have been developed, such as in encompass organic dyes [1], quantum dot [1,3], Raman spectroscopy [1,4], and scanning thermal microscopes [5]. However, those methods have their own limitations such as fluorescence blinking and bleaching, low sensitivity, and large random errors coming from fluorescence rate fluctuations [1–5]. To solve those limitations, quantum sensors based on solid-state spins such as the negatively charged nitrogen-vacancy (N-V^-) center in diamonds [2,6–8] and defects in silicon carbide (SiC) [9,10] have attracted considerable interest recently.

The N-V^- center is usually excited with a 532-nm laser and its fluorescence lies from 600 to 800 nm. Light at these wavelengths will cause more optical damage to living biological systems [11,12]. Moreover, since the biological systems have a noisy environment, it is better to develop a self-protected method to detect the local temperature. To this end, in this paper, we present a self-protected thermometry method based on the neutral divacancy-defects spin in 4H-SiC, with its both excitation and fluorescence wavelength in the infrared (IR) spectral region [13–18]. As compared with the N-V^- center in diamond, highly sensitive thermometry based on a semiconductor material SiC is more fascinating because of its versatility in production and wide application in the realm of electronic and electromechanical devices [13,19]. Moreover, unlike the N-V^- center which has four orientations in bulk diamond [20], one type of divacancy spins in silicon carbide has the same orientation which improves the sensitivity in variations of the sensing application by using an ensemble of divacancy spins [13,14]. Last, there are six distinct forms of the divacancies both in 4H-SiC (named PL1-PL6) and 6H-SiC (named QL1-QL6) [13,14]. They have attracted great interest in recent years as versatile solid-state qubits due to their excellent properties, such as an easy fabrication process, biocompatibility, and long spin coherence and relaxation times (∼ms) [13–16]. These remarkable properties have been explored in many applications such as coherent control [16], quantum registers [15], and quantum sensing such as magnetic sensing [14], electric sensing [17,18], and mechanic sensing [17].

In this paper, we demonstrate a self-protected thermometry based on the divacancies of electron spins in 4H-SiC. First, we theoretically demonstrate that the Ramsey fringe of the divacancy electron spins is robust against magnetic noise due to a self-protected mechanism from the intrinsic

*Corresponding author.
jianmingcai@hust.edu.cn
†Corresponding author.
wbgao@ntu.edu.sg

transverse strain of the defect. Then, we measure the optically detected magnetic resonance (ODMR) with a temperature ranging from about 20 to 300 K, and find its zero-field-splitting (ZFS) parameter D decreases linearly as the temperature increases in the room-temperature range. With these observations, we experimentally demonstrate a self-protected infrared thermometry based on Ramsey methods with the sensitivity about 205.6 $\mathrm{mK/Hz^{1/2}}$. This method provides an appealing route for a real noisy environment, especially in the biological system and microelectronics systems.

II. THEORETICAL MODEL

Here, we consider the PL5 divacancy defect in 4H-SiC [13,14], which is a basal C_{1h} symmetry divacancy showing a high ODMR contrast at room temperature [13]. The ground state shows a spin-1 character with the basis written as $\{|\uparrow\rangle, |0\rangle|\downarrow\rangle\}$. The three ground states split at zero magnetic field, resulting in a two-ODMR resonance spectrum at $D+E$ and $D-E$. The spin Hamiltonian can be written as

$$H = H_0 + H', \tag{1}$$

where

$$H_0 = \hbar D(T) S_z^2 + \hbar E_x (S_x^2 - S_y^2), \tag{2}$$

$$H' = g\mu_B B_z S_z + d_z \prod_z S_z^2. \tag{3}$$

For the H_0 term, $D(T)$ is the temperature-dependence zero field splitting, E_x is the transverse strain due to the lower symmetric of basal defect [13,14], and $S_{x,y,z}$ represents the electronic spin operator. The eigenstates of H_0 are $|\pm\rangle = \frac{1}{2}(|\uparrow\rangle \pm |\downarrow\rangle)$, and $|0\rangle$, with corresponding eigenvalues $D \pm E_x$, 0. For the H' term, $g = 2.00$ is the electron g factor, μ_B is the Bohr magneton, and B_z represents the external magnetic-field fluctuation. In addition, we also consider the electric field fluctuation as denoted as $\prod_z$ [21,22].

On the basis of $\{\uparrow, 0, \downarrow\}$, the initial Hamiltonian $H = H_0 + H'$ can be written in the matrix form

$$H = \hbar \begin{bmatrix} D + \Pi_z' + B_z' & 0 & E_x \\ 0 & 0 & 0 \\ E_x & 0 & D + \Pi_z' - B_z' \end{bmatrix}, \tag{4}$$

where $B_z' = [(g\mu_B)/h]B_z$, $\Pi_z' = (d_z/h)\Pi_z$.

In the thermometry sensing experiment as demonstrated in this article, the applied external microwave is almost on resonant with the transition 0 and $|+\rangle$ (with detuning Δ). Therefore, the Hamiltonian can be shown more clearly in the basis $\{+,0,-\}$, where $|+\rangle = \frac{1}{2}(|\uparrow\rangle + |\downarrow\rangle)$; $|-\rangle = \frac{1}{2}(|\uparrow\rangle - |\downarrow\rangle)$. The total Hamiltonian in the basis of $\{+,0,-\}$, adding the microwave term can be rewritten as

$$H_{dr,\pm} = \hbar \begin{bmatrix} D + \prod_z' + E_x & \Omega\cos\omega t & B_z' \\ \Omega\cos\omega t & 0 & 0 \\ B_z' & 0 & D + \prod_z' + E_x \end{bmatrix}, \tag{5}$$

where Ω is the Rabi frequency of microwave. As can be seen, the microwave would only drive the transition between $|0\rangle$ and $|+\rangle$, while $|-\rangle$ is decoupled. The Hamiltonian under rotating wave approximation [23] can be written as

$$H_{\mathrm{rot},\pm} = \hbar \begin{bmatrix} \Delta + \Pi_z' & \Omega & B'_z \\ \Omega & 0 & 0 \\ B_z' & 0 & \Delta + \Pi_z' - 2E_x \end{bmatrix}. \tag{6}$$

Here, $\Delta = D + E_x - \omega$. Going back to the basis $\{|\uparrow\rangle, |0\rangle, |\downarrow\rangle\}$, the total Hamiltonian becomes

$$H_{\mathrm{rot}} = \hbar \begin{bmatrix} \Delta + \Pi_z' - E_x + B_z' & \frac{\Omega}{\sqrt{2}} & E_x \\ \frac{\Omega}{\sqrt{2}} & 0 & \frac{\Omega}{\sqrt{2}} \\ E_x & \frac{\Omega}{\sqrt{2}} & \Delta + \Pi_z' - E_x - B_z' \end{bmatrix}. \tag{7}$$

To perform the measurement of temperature, we adopt a Ramsey scheme. We first initialize the spin into the state $|0\rangle$, and apply a $\pi/2$ pulse to drive the system into the superposition state of $|0\rangle$ and $|+\rangle$ with equal amplitude: $U_{\pi/2}|0\rangle = (1/\sqrt{2})(|0\rangle - i|+\rangle)$. After a free evolution for time τ, we apply another $\pi/2$ pulse to map the phase information to the state population.

When the microwave is off, the Hamiltonian is

$$H_{\mathrm{rot}}(0) = h \begin{bmatrix} \Delta + \Pi_z' - E_x + B_z' & 0 & E_x \\ 0 & 0 & 0 \\ E_x & 0 & \Delta + \Pi_z' - E_x - B_z' \end{bmatrix}. \tag{8}$$

Assuming that Ω is much larger than Δ, B_z', Π_z', and the pulse lengths are much shorter than the free evolution time, the terms including Δ, B_z', Π_z' can be neglected during the pulse operations. When the microwave is on, the Hamiltonian in basis $\{\uparrow, 0, \downarrow\}$ can be written as

$$H_{\mathrm{rot}}(\Omega) = \hbar \begin{bmatrix} -E_x & \frac{1}{\sqrt{2}}\Omega & E_x \\ \frac{1}{\sqrt{2}}\Omega & 0 & \frac{1}{\sqrt{2}}\Omega \\ E_x & \frac{1}{\sqrt{2}}\Omega & -E_x \end{bmatrix}. \tag{9}$$

For an initial state $|0\rangle$, we first apply a $\pi/2$ pulse $U_{\pi/2} = e^{-i(\pi/4\Omega)H_{\rm rot}(\Omega)/\hbar}$ that drives the system to the superposition state of $|0\rangle$ and $|+\rangle$:

$$U_{\pi/2}|0\rangle = \frac{1}{\sqrt{2}}(|0\rangle - i|+\rangle). \tag{10}$$

Then, the system undergoes a free evolution for time τ represented by the operator $U_{\pi/2} = e^{-iH_{\rm rot}(0)\tau/\hbar}$. The state becomes

$$\begin{aligned} U_\tau U_{\pi/2}|0\rangle = &\frac{1}{\sqrt{2}}|0\rangle + \frac{e^{-2\pi i(\Delta+\Pi'_z-E_x)\tau}}{2i} \\ &\times\left[\left(\cos 2\pi\delta\tau - \frac{E_x+B'_z}{\delta} i\sin 2\pi\delta\tau\right)|\uparrow\rangle\right. \\ &\left.+\left(\cos 2\pi\delta\tau - \frac{E_x-B'_z}{\delta} i\sin 2\pi\delta\tau\right)|\downarrow\rangle\right], \end{aligned} \tag{11}$$

where $\delta = \sqrt{E_x^2 + B'^2_z} \approx E_x[1 + (B'^2_z/2E_x^2)]$. Finally, we apply another $\pi/2$ pulse for measurement. The final amplitude of state $|0\rangle$ can be calculated by $A_{0,\rm final} = \frac{1}{2} - (i/2)(A'_\uparrow + A'_\downarrow)$, where $A'_\uparrow(A'_\downarrow)$ is the amplitude of $|\uparrow\rangle(|\downarrow\rangle)$ before the final $\pi/2$ rotation. If one neglects terms higher than $O(B'_z/E_x)$, it becomes

$$A_{0,\rm final} = \frac{1}{2}(1 - ie^{-2\pi i[\Delta+\Pi'_z+(B'^2_z/2E_x)]\tau}), \tag{12}$$

and the value of final population of the $|0\rangle$ state is

$$P'_{0,\rm final} = \frac{1}{2} - \frac{1}{2}\cos 2\pi\left(\Delta + \Pi'_z + \frac{B'^2_z}{2E_x}\right)\tau. \tag{13}$$

The oscillation of P'_0 is dominated by the detuning $P'_{0,\rm final} = \frac{1}{2} - \frac{1}{2}\cos 2\pi[(\Delta + \Pi'_z + B'^2_z/2E_x)]\tau$, $\Delta = D(T) + E_x - \omega$. Since $D(T)$ changes with temperature, the change of the oscillation frequency of P'_0 can be used to determine the change of temperature.

The sensitivity for the measurement of temperature is determined by the coherence time of the spin sensor. The main noise that would affect the coherence time in the present experiment is the external magnetic-field fluctuation. In the free evolution step, the unexpected B'_z has opposite effects on spin $\uparrow$ and $\downarrow$ by giving a positive or negative phase for the $|\uparrow\rangle$ or $|\downarrow\rangle$ state. As can be seen from the Hamiltonian in Eq. (7), one of the effects of transverse strain is to flip the $|\uparrow\rangle$ and $|\downarrow\rangle$ continuously. Therefore, the direction of the magnetic field experienced by the electron spin is changing continuously. If the strain is large enough, the effect induced by the environment noise B'_z is reduced to the order of $O(B'^2_z/E_x)$, as compared with $O(B'_2)$ when E_x is negligible [6]. This provides a self-protected mechanism even without requiring an extra operation as conventional active dynamical decoupling schemes.

III. EXPERIMENTAL SETUP

The sample is a bulk high-quality semi-insulating 4*H*-SiC purchased from CREE. In the experiment, we use a homebuild confocal system combined with a microwave system [Figs. 1(a) and 1(b)]. A 950-nm IR laser focuses on the sample through an infrared objective with NA of 0.8. The fluorescence above 1000 nm is collected and guided through a multimode fiber to an infrared photon

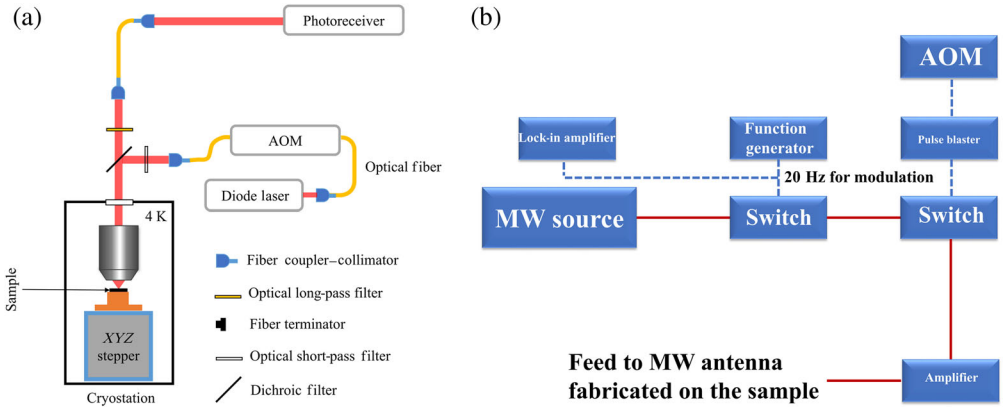

FIG. 1. (a) Schematic figure of a homebuilt confocal microcopy system. (a) A 950-nm infrared diode laser is used to excite the defects though an infrared objective with NA of 0.8. The photoluminescence from PL5 is collected from the same objective and coupled to a photoreceiver (Femto, OE-200-IN1). The sample is mounted on the *xyz* steppers in the Montana Cryostation (4–300 K). At room experiment, we use another confocal system which is the same with the low temperature. The sample is mounted on a resistive heater (Thorlabs, TEC3-2.5) for temperature control and a thermistor (Thorlabs, HT10K) is attached to measure the temperature. (b) Schematic figure of the microwave system. The microwave first went through two switches, one is for 20-Hz modulation and the other one is for fast spin control by pulse plaster. The output of the photoreceiver is sent to a lock-in amplifier (Stanford Research System SR830) for lock-in detection.

receiver. As a rough estimation, by converting the output voltage of our Femto receiver to photon counts and assuming that all types of divacancy have the same brightness, in the 1 μm in xy plane and 3 μm in the z-direction sensing volume, we have addressed 1.4-k PL5 defects and the defect density is around 5.8×10^{20} m^3. To manipulate the spin state, the microwave with a tunable frequency is fed to the sample through a microwave antenna fabricated on the sample. The antenna (Au/Pt) has a ring-shape structure with 80-μm inner diameter. To reduce the microwave noise, we modulate the microwave with a frequency of 20 Hz using a microwave switch and the same signal is used for lock-in detection of the fluorescence from the defects.

IV. RESULTS AND DISCUSSION

A. ODMR measurement

With the setup described, we first characterize the ODMR frequency of the divacancy defects. As shown in Fig. 2(a), lower panel, different microwave frequency peaks are observed in the ODMR spectrum at zero magnetic field. To further identify these peaks, we measured the ODMR spectrum as a function of the applied magnetic field in the z direction, as shown in Fig. 2(a), upper panel. Because of the different symmetry property of the defects, these ODMR resonances show a different diverging behavior. For example, at zero magnetic field, two resonance transitions of the c-axis divacancy have a small splitting. When there is a static magnetic field along the c axis, two transitions split at the slope of 2.8 MHz/G, as marked using the dashed line in the figure. This shows the same behavior as the N-V^- center [20]. For these transitions, we identify them as PL6. While for C_{1h} symmetry PL5, two resonance transitions will bend and the left branch of the PL5 resonance is mixed with PL7 and the right branch is alone. All thermometry experiment in this paper is based on the right-branch resonant transition of PL5 ($|0\rangle \leftrightarrow |+\rangle$) because it is well isolated with other transitions.

Next, we proceed to measure the temperature dependence of the ODMR spectrum. Because of thermal expansion and electron-phonon interactions, transition-resonance frequencies tend to increase when the temperature decreases [24]. In the ODMR spectrum scan shown in Fig. 2(b), all transitions of PL5 to PL7 exhibit a similar

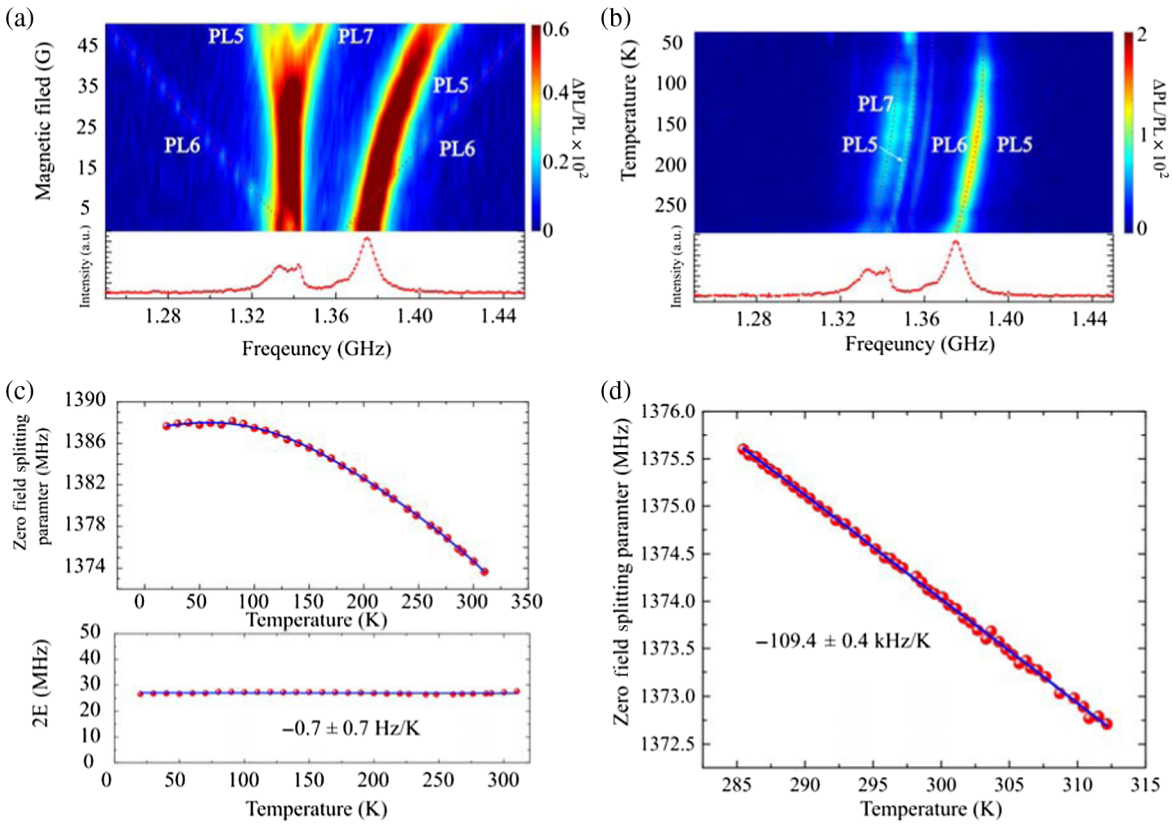

FIG. 2. (a) Room-temperature ODMR spectrum map of 4H-SiC divacancy spins PL5 with respect to the B field along the c axis. Lower panel shows a line cut at zero magnetic field. PL5, PL6, and PL7 represent different defect types in SiC. (b) ODMR spectrum map as a function of temperature. Dashed line is drawn as a guide for the eye. Lower panel shows a line cut at 300 K. (c) Upper panel: ZFS (zero field splitting) parameter shift for the PL5 right branch ODMR spectrum as a function of temperature. Lower panel: Transverse components of the PL5 ZPL with respect to the temperature, which shows that it stays roughly in a constant level. (d) ZFS shift at near room temperature. A linear shift is used for the fitting.

behavior, which shows that such a resonance-frequency shift is their intrinsic property. The temperature dependence of the PL5 ZFS parameter D ranging from 20 to 300 K is shown in Fig. 2(c) and the nonlinear shift is fitted with a fifth-order polynomial. The transverse strain E_x (13.5 ± 0.048 MHz) is also estimated from the difference between the left branch ($D - E_x$) and right branch ($D + E_x$). By linear fitting with a slope of -0.7 Hz/K, it indicates that the transversal component $2E_x$ does not have an obvious shifting, and the shifting of the ZFS is mainly due to the axial component D, which shows the same behavior as the N-V^- center in diamond [22]. In order to get a more detailed shifting of the D value with respect to the temperature, we measure the ODMR resonance of the PL5 right branch ($D + E_x$) near room temperature [Fig. 2(d)]. It follows a good linear relationship with respect to the temperature at a slope of $dD/dT = -109.4 \pm 0.4$ kHz/K, which indicates a thermal shift of OMDR transition in PL5 more than N-V^- centers in diamond ($dD/dT - 74.2$ kHz/K) [25].

B. Coherent control

The frequency shift of ZFS shown above indicates that SiC divacancies can be potentially used as a temperature sensor by using Ramsey interferometry. As a first step, we demonstrate the coherent control of electron spins (Fig. 3). The pulse sequence for Rabi oscillation and the Ramsey fringe is shown in Fig. 3(a). First, a 2-μs $\pi/2$ pulse is used to initialize the spin. Following the initialization pulse, the 20-Hz modulated Rabi or Ramsey microwave pulse is applied to coherently manipulate the spin state. Finally, the spin state is read out by another 2 μs $\pi/2$ pulse. The population change of the final state will result in a change of PL intensity ΔPL, which is detected with a lock-in method. Figures 3(b) and 3(c) show Rabi oscillations and Ramsey fringes, respectively, when the temperature is 210 K. The Ramsey fringes are fitted with the equation

$$I = a \exp\left[-\left(\frac{t}{T_2^*}\right)^n\right] \cos(2\pi f t + \varphi) + b, \qquad (14)$$

where a, n, φ, and b are free parameters, t is the evolution time, and T_2^* is the dephasing time. The oscillation of the Ramsey measurement is induced by a microwave with a detuning of 2 MHz from resonance. The spin-dephasing time T_2^* is a critical factor in the dc-magnetic sensing and temperature sensing [6,26,27]. For each temperature, we measure the Ramsey fringes and extract T_2^* as shown in Fig. 3(d). The result shows that T_2^* remains almost constant at around 2 μs at the temperature ranging from 50 to 300 K.

Next, we demonstrate thermometry based on the Ramsey fringes method. The frequency of Ramsey fringes is induced by detuning Δ. As explained above, the temperature shift will result in a linear change of the D value as shown in Fig. 3(d), which is directly related to the oscillations frequency of the Ramsey fringes. As shown in the Fig. 4(a), Ramsey measurement of PL5 shows good oscillations without strong coupling with other unwanted nuclear spins. The data are fitted with Eq. (14). Figure 4(b) displays the Ramsey oscillation frequency and follows a good liner relationship with respect to the temperature change. The slope -108.2 ± 0.5 kHz/K also matches with the measured temperature dependence shift -109.4 ± 0.4 kHz/K of the D value obtained from the ODMR resonance spectrum.

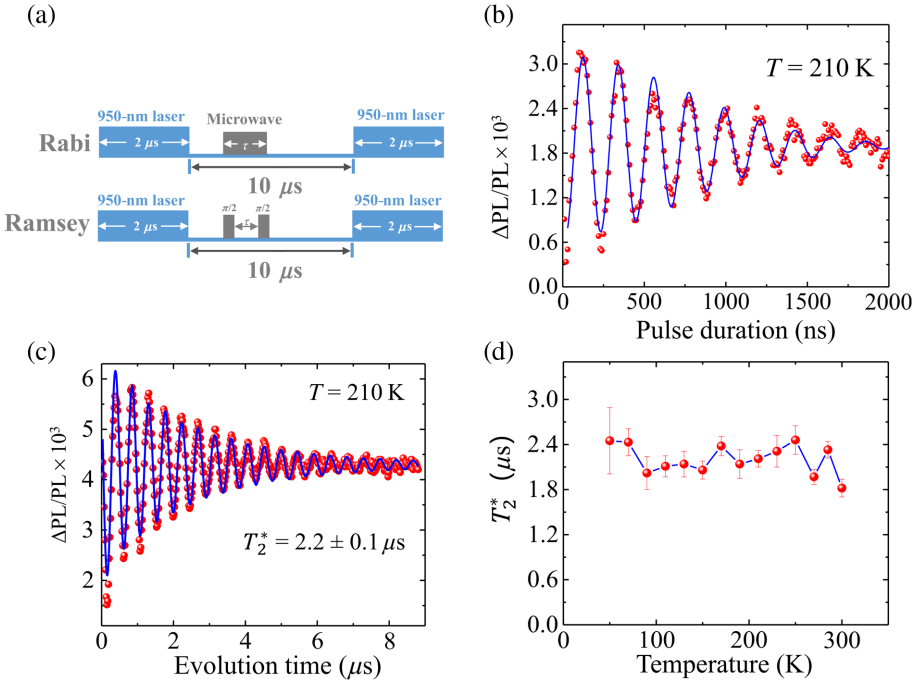

FIG. 3. (a) Rabi and Ramsey pulse sequence. A 950-nm laser pulse is used for spin initialization and spin readout. One microwave pulse with a variable pulse length is used for the Rabi oscillation measurement. Two $\pi/2$ pulses with a variable delay are used for Ramsey fringes. (b) Rabi oscillation of PL5. Fluorescence change has been recorded as a function of microwave pulse length. A decayed sinuous function is used to fit the experimental data. The measurement is performed at temperature 210 K. (c) Ramsey fringe. The microwave frequency has a detuning of 2 MHz with respect to the resonance frequency. The oscillations show decayed sinuous oscillation with a period of 500 ns. The decay time shows that the dephasing time T_2^* is 2.2 μs. (d) Inhomogeneous dephasing time with respect to temperature.

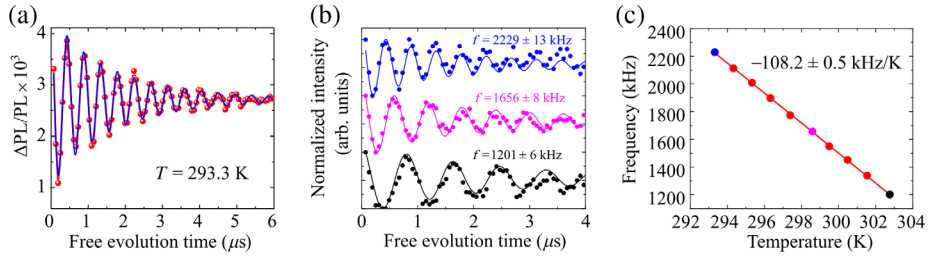

FIG. 4. (a) Ramsey fringes at 293.3 K. Oscillation is fitted with Eq. (14). (b) Ramsey oscillation at three different temperatures. The fitted f value is given above each curve. (c) Ramsey oscillation frequency $\Delta(T) = D(T) + E_x - \omega$ as a function of temperature when the microwave frequency ω is fixed. $\Delta(T)$ is fitted with a linear function with a slope of -108.2 ± 0.5 kHz/K. Three points in (b) are marked as the same color (blue, pink, and black).

The Ramsey-based method can be applied to a wide range of temperatures, as shown in Fig. 2(c). The thermal sensitivity η has an estimated value of about 205.6 mK/Hz$^{1/2}$. The sensitivity can be derived using [6,28]

$$\eta = \sqrt{\frac{2(p_0 + p_1)}{(p_0 - p_1)^2}} \frac{1}{2\pi \frac{dD}{dT} \exp[-(\frac{t}{T_2^*})^n] \sqrt{t}}, \qquad (15)$$

where p_0 and p_1 are the photon counts per measurement shot for the bright and dark spin states, respectively. t is the measurement time. The η value given in the main text corresponds to the maximum value of $\exp[-(t/T_D)^n]\sqrt{t}$. The sensitivity is less than an order of magnitude than Ref. [2]. The reason is the contrast of Ramsey $(1 - p_0/p_1)$ is around 20% ∼ 30% [6] for N-V^- centers in diamond, while in our case, the contrast is only 0.23%. Now, the low contrast 0.23% is partly caused by off-resonant excitation of other unwanted defects (PL1 to PL4, PL6, and PL7). One way to get rid of unwanted photoluminescence from other types of defects and to increase the ODMR contrast is to perform resonant excitation and only selectively excite PL5.

C. Thermal echo measurement

One of the most widely used dynamically decoupled schemes for thermometry is the thermal echo (TE) sequence [2]. TE is the Ramsey pulse sequence adding a 2π pulse in the middle of free evolution. With this extra 2π pulse, states $|\uparrow\rangle$ and $|\downarrow\rangle$ exchange their population, making the asymmetric phase accumulation of the $B'_z S_z$ term before and after the 2π rotation cancel each other. For the N-V^- center in diamond, TE can increase T_2^* by at least an order of magnitude as compared to Ramsey measurement. In our system of PL5 divacancy in SiC, however, the coherence time is not expected to increase with TE, because the effect of B'_z has already been suppressed for Ramsey measurement.

We experimentally test the TE pulse sequence for thermometry. As shown in Fig. 5(a), the extracted coherence time is 2.3 μs, which is in the same order of the dephasing time for the Ramsey sequence. This agrees well with our theoretical model. The frequency follows a good linear relationship with the temperature change, which is in Fig. 5(b). The slope -108 ± 1 kHz/K again matches with the temperature dependence of the D value very well.

D. Self-protection effect

As described in the previous sections, the defect types we are using have a large transverse strain E_x, which will protect the temperature sensor against the environment magnetic-field noise. We experimentally verify such a self-protection mechanism as provided by E_x. In the experiment, we vary the magnetic field around the sample with a randomly changed value between $-B$ to B (where B is the maximum amplitude of the magnetic-field fluctuation) at a frequency of 100 Hz, and then observe how the Ramsey oscillation decay changes, which represents the effect of the magnetic field fluctuation on T_2^*.

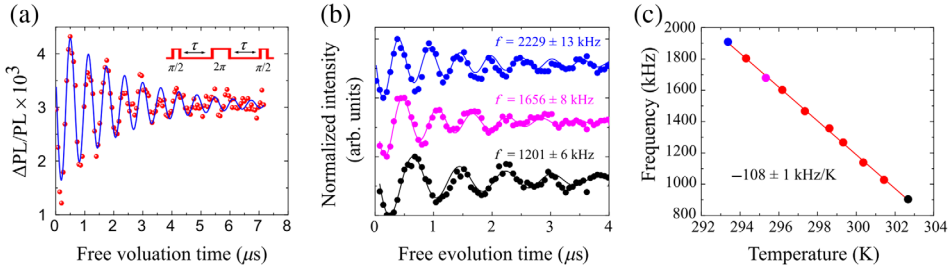

FIG. 5. (a) TE sequence at room temperature. Red dots are the raw data and the blue curve is the fitting with Eq. (14). (b) TE sequence at three different temperatures, fitted f value is given above each curve. (c) Frequency at ten different temperatures. It is fitted with a linear function (red curve) with a slope of -108.2 ± 1 kHz/K. Three points in (b) are marked as the same color (blue, pink, and black).

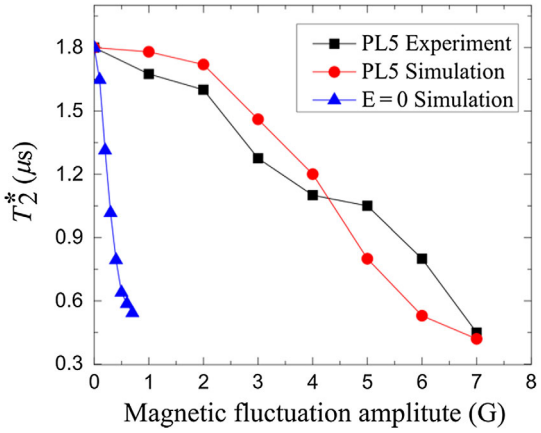

FIG. 6. The relationship between T_2^* and the magnetic fluctuation amplitude (black dot for experiment data; red and blue dot for simulation). For the PL5 defect with $E = 13.5$ MHz, T_2^* decays slower than the case when $E = 0$, which shows the self-protect effect by the large E_x in SiC PL5 defects.

In Fig. 5, both experimental and numerical results of T_2^* for different applied ac magnetic fields have been shown. The simulation is done with the Hamiltonian equation (4) following the Ramsey pulse sequence discussed in previous sections. In our experiment, the magnetic field can only be applied perpendicular to the sample. Since the c axis of PL5 is at 109.5° from the normal of the sample [17], B_z' in Eq. (13) should be $B_z' = \cos(109.5°)B_{\text{applied}}$, where B_{applied} is the total amplitude of the magnetic field applied by an electronic magnet. There are two random parameters in Eq. (13), namely Π_z' and B_z'. For Π_z', we assume it follows the standard normal distribution with the zeros' average value. The standard deviation $\sigma_{\Pi_z'}$ is determined by the experimental result $T^*_{2,B_z=0} = 1.8$ μs when $B_{\text{applied}} = 0$ MHz. When the magnetic-field fluctuation is negligible, one has the relation [21]: $T^*_{2,B=0} = 1/(\sqrt{2}\pi\sigma_{\Pi_z'})$. For B_z', we assume it to be white noise between the maximum ($+B$) and minimum ($-B$) allowed value. For each value of B, we average the evolution of 1000 times of run for different randomly chosen Π_z' and B_z'. The value of T_2^* is obtained by the fitting of the average evolution.

Our theoretical simulation as shown in red dots (Fig. 6) matches the experimental data quite well. The detailed simulation method and result is shown in Supplemental Material [29]. When $E_x = 0$, T_2^* decreases dramatically for small amplitude as shown in the simulation. We note that this agrees with the previous experimental results based on the N-V^- center in diamond, where T_2^* is found to be very sensitive to the magnetic field perturbation [21]. Both the simulation and experimental data support our observation that the intrinsic nonzero strain E enables a self-protected mechanism for the electron spin coherence against the magnetic-field noise and therefore sustains a high sensitivity of the present temperature sensing.

V. CONCLUSIONS

In summary, we have demonstrated infrared SiC thermometry based on the coherence of electron spins with the Ramsey pulse sequence. Especially, they are protected by the intrinsic large transverse strain of the defects, which simplifies the procedure for protecting the sensor sensibility. It is to be expected that by using dynamical decoupling [13,30], isotopically pure SiC [31], and techniques of higher photon collection efficiency, such as solid immersion lenses [32], nanopillars [33], the thermal sensitivity can be further improved. Silicon carbide itself is biocompatible and the required infrared laser beam in this thermometry sensing would cause less damage than the visible beam to the biosystem [12]. This technique can be applied to the thermometry of a living cell if SiC nanoparticles [34,35] are used, which is similar to the nanodiamond case [2]. Moreover, combining this method with the SiC nanoparticles and atomic force microscope (AFM), it can realize the nanoscale thermal image [36].

ACKNOWLEDGMENTS

We acknowledge the support from the Singapore National Research Foundation fellowship grant (No. NRF-NRFF2015-03) and its Competitive Research Program (CRP Award No. NRF-CRP14-2014-02), Astar QTE project, Singapore Ministry of Education (No. MOE2016-T2-2-077, No. MOE2017-T2-1-163, and No. RG176/15) and a start-up grant (No. M4081441) from Nanyang Technological University. J.-M. C. is supported by the National Natural Science Foundation of China (Grant No. 11574103).

Y. Z., J. W., and X. Z. contributed equally to this work.

[1] C. D. S. Brites, P. P. Lima, N. J. O. Silva, A. Millan, V. S. Amaral, F. Palacio, and L. D. Carlos, Thermometry at the nanoscale, Nanoscale **4**, 4799 (2012).

[2] G. Kucsko, P. C. Maurer, N. Y. Yao, M. Kubo, H. J. Noh, P. K. Lo, H. Park, and M. D. Lukin, Nanometre-scale thermometry in a living cell, Nature (London) **500**, 54 (2013).

[3] G. W. Walker, V. C. Sundar, C. M. Rudzinski, A. W. Wun, M. G. Bawendi, and D. G. Nocera, Quantum-dot optical temperature probes, Appl. Phys. Lett. **83**, 3555 (2003).

[4] A. A. Balandin, S. Ghosh, W. Bao, I. Calizo, D. Teweldebrhan, F. Miao, and C. N. Lau, Superior thermal conductivity of single-layer grapheme, Nano Lett. **8**, 902 (2008).

[5] A. Majumdar, Scanning thermal microscopy, Annu. Rev. Mater. Sci. **29**, 505 (1999).

[6] D. M. Toyli, C. F. de las Casas, D. J. Christle, V. V. Dobrovitski, and D. D. Awschalom, Fluorescence thermometry enhanced by the quantum coherence of single spins in diamond, Proc. Natl. Acad. Sci. U.S.A. **110**, 8417 (2013).

[7] P. Neumann, I. Jakobi, F. Dolde, C. Burk, R. Reuter, G. Waldherr, J. Honert, T. Wolf, A. Brunner, J. H. Shim, D. Suter, H. Sumiya, J. Isoya, and J. Wrachtrup, High-precision

nanoscale temperature sensing using single defects in diamond, Nano Lett. **13**, 2738 (2013).

[8] J. F. Wang, F. P. Feng, J. Zhang, J. H. Chen, Z. C. Zheng, L. P. Guo, W. L. Zhang, X. R. Song, G. P. Guo, L. L. Fan, C. W. Zou, L. R. Lou, W. Zhu, and G. Z. Wang, High-sensitivity temperature sensing using an implanted single nitrogen-vacancy center array in diamond, Phys. Rev. B **91**, 155404 (2015).

[9] H. Kraus, V. A. Soltamov, F. Fuchs, D. Simin, A. Sperlich, P. G. Baranov, G. V. Astakhov, and V. Dyakonov, Magnetic field and temperature sensing with atomic-scale spin defects in silicon carbide, Sci. Rep. **4**, 5303 (2014).

[10] A. N. Anisimov, D. Simin, V. A. Soltamov, S. P. Lebedev, P. G. Baranov, G. V. Astakhov, and V. Dyakonov, Optical thermometry based on level anticrossing in silicon carbide, Sci. Rep. **6**, 33301 (2016).

[11] K. König, H. Liang, M. W. Berns, and B. J. Tromberg, Cell damage in near-infrared multimode optical traps as a result of multiphoton absorption, Opt. Lett. **21**, 1090 (1996).

[12] A. Ashkin, J. M. Dziedzic, and T. Yamane, Optical trapping and manipulation of single cells using infrared laser beams, Nature (London) **330**, 769 (1987).

[13] W. F. Koehl, B. B. Buckley, F. J. Heremans, G. Calusine, and D. D. Awschalom, Room temperature coherent control of defect spin qubits in silicon carbide, Nature (London) **479**, 84 (2011).

[14] A. L. Falk, B. B. Buckley, G. Calusine, W. F. Koehl, V. V. Dobrovitski, A. Politi, C. A. Zorman, P. X.-L. Feng, and D. D. Awschalom, Polytype control of spin qubits in silicon carbide, Nat. Commun. **4**, 1819 (2013).

[15] Paul. V. Klimov, A. L. Falk, D. J. Christle, V. V. Dobrovitski, and D. D. Awschalom, Quantum entanglement at ambient conditions in a macroscopic solid-state spin ensemble, Sci. Adv. **1**, e1501015 (2015).

[16] H. Seo, A. L. Falk, P. V. Klimov, K. C. Miao, G. Galli, and D. D. Awschalom, Quantum decoherence dynamics of divacancy spins in silicon carbide, Nat. Commun. **7**, 12935 (2016).

[17] A. L. Falk, P. V. Klimov, B. B. Buckley, V. Ivády, I. A. Abrikosov, G. Calusine, W. F. Koehl, A. Gali, and D. D. Awschalom, Electrically and Mechanically Tunable Electron Spins in Silicon Carbide Color Centers, Phys. Rev. Lett. **112**, 187601 (2014).

[18] P. V. Klimov, A. L. Falk, B. B. Buckley, and D. D. Awschalom, Electrically Driven Spin Resonance in Silicon Carbide Color Centers, Phys. Rev. Lett. **112**, 087601 (2014).

[19] C. M. Zetterling, *Process Technology for Silicon Carbide Devices* (IET, London, 2002).

[20] M. W. Doherty, N. B. Manson, P. Delaney, F. Jelezko, J. Wrachtrup, and L. C. L. Hollenberg, The nitrogen-vacancy colour centre in diamond, Phys. Rep. **528**, 1 (2013).

[21] P. Jamonneau, M. Lesik, J. P. Tetienne, I. Alvizu, L. Mayer, A. Dréau, S. Kosen, J.-F. Roch, S. Pezzagna, J. Meijer, T. Teraji, Y. Kubo, P. Bertet, J. R. Maze, and V. Jacques, Competition between electric field and magnetic field noise in the decoherence of a single spin in diamond, Phys. Rev. B **93**, 024305 (2016).

[22] F. Dolde, H. Fedder, M. W. Doherty, T. Nöbauer, F. Rempp, G. Balasubramanian, T. Wolf, F. Reinhard, L. C. L. Hollenberg, F. Jelezko, and J. Wrachtrup, Electric-field sensing using single diamond spins, Nat. Phys. **7**, 459 (2011).

[23] J. S. Hodges, N. Y. Yao, D. Maclaurin, C. Rastogi, M. D. Lukin, and D. Englund, Time keeping with electron spin states in diamond, Phys. Rev. A **87**, 032118 (2013).

[24] X.-D. Chen, C.-H. Dong, F.-W. Sun, C.-L. Zou, J.-M. Cui, Z.-F. Han, and G.-C. Guo, Temperature dependent energy level shifts of nitrogen-vacancy centers in diamond, Appl. Phys. Lett. **99**, 161903 (2011).

[25] V. M. Acosta, E. Bauch, M. P. Ledbetter, A. Waxman, L. S. Bouchard, and D. Budker, Temperature Dependence of the Nitrogen-Vacancy Magnetic Resonance in Diamond, Phys. Rev. Lett. **104**, 070801 (2010).

[26] M. W. Doherty, V. V. Struzhkin, D. A. Simpson, L. P. McGuinness, Y. Meng, A. Stacey, T. J. Karle, R. J. Hemley, N. B. Manson, L. C. L. Hollenberg, and S. Prawer, Electronic Properties and Metrology Applications of the Diamond NV^- Center under Pressure, Phys. Rev. Lett. **112**, 047601 (2014).

[27] J. M. Taylor, P. Cappellaro, L. Childress, L. Jiang, D. Budker, P. R. Hemmer, A. Yacoby, R. Walsworth, and M. D. Lukin, High-sensitivity diamond magnetometer with nanoscale resolution, Nat. Phys. **4**, 810 (2008).

[28] D. M. Toyli, D. J. Christle, A. Alkauskas, B. B. Buckley, C. G. Van de Walle, and D. D. Awschalom, Measurement and Control of Single Nitrogen-Vacancy Center Spins above 600 K, Phys. Rev. X **2**, 031001 (2012).

[29] See Supplemental Material at http://link.aps.org/supplemental/10.1103/PhysRevApplied.8.044015 for additional details of the simulation.

[30] D. Simin, H. Kraus, A. Sperlich, T. Ohshima, G. Astakhov, and V. Dyakonov, Locking of electron spin coherence above 20 ms in natural silicon carbide, Phys. Rev. B **95**, 161201 (2017).

[31] D. Simin *et al.*, All-Optical dc Nanotesla Magnetometry Using Silicon Vacancy Fine Structure in Isotopically Purified Silicon Carbide, Phys. Rev. X **6**, 031014 (2016).

[32] M. Widmann, S.-Y. Lee, T. Rendler, N. T. Son, H. Fedder, S. Paik, L.-P. Yang, N. Zhao, S. Yang, I. Booker, A. Denisenko, M. Jamali, S. A. Momenzadeh, I. Gerhardt, T. Ohshima, A. Gali, E. Janzén, and J. Wrachtrup, Coherent control of single spins in silicon carbide at room temperature, Nat. Mater. **14**, 164 (2015).

[33] M. Radulaski *et al.* Scalable quantum photonics with single color centers in silicon carbide, Nano Lett. **17**, 1782 (2017).

[34] S. Castelletto, B. C. Johnson, C. Zachreson, D. Beke, I. Balogh, T. Ohshima, I. Aharonovich, and A. Gali, Room temperature quantum emission from cubic silicon carbide nanoparticles, ACS Nano **8**, 7938 (2014).

[35] A. Muzha, F. Fuchs, N. V. Tarakina, D. Simin, M. Trupke, V. A. Soltamov, E. N. Mokhov, P. G. Baranov, V. Dyakonov, A. Kruegerand, and G. V. Astakhov, Room-temperature near-infrared silicon carbide nanocrystalline emitters based on optically aligned spin defects, Appl. Phys. Lett. **105**, 243112 (2014).

[36] A. Laraoui, Aycock-Rizzo, Y. Gao, X. Lu, E. Riedo, and C. A. Meriles, Imaging thermal conductivity with nanoscale resolution using a scanning spin probe, Nat. Commun. **6**, 8954 (2015).